PNAS RESEARCH ARTICLE | BIOCHEMISTRY

# Hyperpolarized [5-$^{13}$C,4,4-$^{2}H_2$,5-$^{15}$N]-L-glutamine provides a means of annotating in vivo metabolic utilization of glutamine

Roozbeh Eskandari[a,b], Nathaniel Kim[a,b], Arsen Mamakhanyan[a,b], Michelle Saoi[c], Guannan Zhang[a,b], Marjan Berishaj[a,b], Kristin L. Granlund[a,b], Alex J. Poot[a,b], Justin Cross[c], Craig B. Thompson[d,1], and Kayvan R. Keshari[a,b,e,1]

Contributed by Craig B. Thompson; received November 17, 2021; accepted April 7, 2022; reviewed by Navdeep Chandel and Julie Sutcliffe

**Glutamine is consumed by rapidly proliferating cells and can provide the carbon and nitrogen required for growth through various metabolic pathways. However, delineating the metabolic fate of glutamine is challenging to interrogate in vivo. Hyperpolarized magnetic resonance, by providing high transient nuclear magnetic resonance signals, provides an approach to measure fast biochemical processes in vivo. Aminohydrolysis of glutamine at carbon-5 plays an important role in providing nitrogen and carbon for multiple pathways. Here, we provide a synthetic strategy for isotope-enriched forms of glutamine that prolongs glutamine-C5 relaxation times and thereby reveals in vivo reactions involving carbon-5. We investigate multiple enrichment states, finding [5-$^{13}$C,4,4-$^{2}H_2$,5-$^{15}$N]-L-glutamine to be optimal for hyperpolarized measurement of glutamine conversion to glutamate in vivo. Leveraging this compound, we explore pancreatic cancer glutamine metabolism in vivo. Taken together, this work provides a means for studying glutamine metabolic flux in vivo and demonstrates on-target effects of metabolic enzyme inhibitors.**

metabolic imaging | magnetic resonance imaging | cancer metabolism | pancreatic cancer

## Significance

Glutamine is the most abundant amino acid in human plasma, although it is challenging to determine glutamine's metabolic fate noninvasively. In this work, we utilize established chemical methods to develop a platform for imaging glutamine metabolism using hyperpolarized magnetic resonance imaging. Using this strategy, we are able to spatially measure glutaminolysis in vivo as well as develop a biomarker for the inhibition of glutaminase. Combining this biomarker with isotope tracing metabolomics connects this inhibition to reduced glutamine contribution to the tricarboxylic acid cycle. This provides an approach for future imaging of glutamine metabolism in humans.

Metabolic biomarkers provide significant insights into organismal physiology and energy homeostasis. Quantitative measurements of the corresponding metabolic pathways can be highly descriptive and provides insights into disease progression. Glutamine is the most abundant amino acid in extracellular fluid and is a source of nitrogen, a potent anaplerotic substrate to maintain the tricarboxylic acid (TCA) cycle, and a precursor in the synthesis of many nonessential amino acids, nucleotides and glycosylated lipids/proteins. Quantification of glutamine metabolism is increasingly recognized as altered in multiple diseases including cancer, diabetes, and neurodegeneration (1–4). Following uptake, glutamine can play a critical role in maintaining multiple enzymatic pathways. For example, within both the cytosol and mitochondria, glutamine can be rapidly converted to glutamate, and this pool mediates TCA cycle anaplerosis through $\alpha$-ketoglutarate (5). Glutamine-derived glutamate can also be used to maintain redox balance through synthesis of glutathione (6, 7). Thus, glutamine supports cellular bioenergetics and redox homeostasis. Alternatively, the amine at carbon-5 can be used to donate nitrogen for the synthesis of nucleotide and glycosylation intermediates. In vitro, some tumor cells exhibit a high level of glutamine catabolism, termed glutaminolysis, where mitochondrial glutaminase (GLS) activity contributes to pyrimidine and proline biosynthesis (8–10).

Due to the relevance of glutamine metabolism in a variety of diseases, ranging from cancer to neurodegeneration (11–13), advances have been made in the setting of therapeutics related to this pathway with the most common strategy being to inhibit flux through glutaminase. It is commonly appreciated that a lack of methods to noninvasively visualize metabolic flux from glutamine through this pathway limits development of therapies, stratification of treatment response, and extend our fundamental understanding of in vivo glutamine metabolism (11). Among the many in vivo probes to assess glutamine metabolism, $^{18}$F-(2S, 4R)-4F-glutamine as a positron-emission tomography probe has widely been used as a noninvasive approach in preclinical models as well as translated to humans (14–17). However, uptake of this probe relies on glutamine transporter activity and is unable to provide further downstream mechanistic insight into metabolic flux. Other magnetic resonance spectroscopic imaging (MRSI) methods have been developed to address glutamine metabolism in vivo, including $^{1}$H MRSI and glutamate-based chemical exchange saturation transfer (18), although these are limited both in spatial resolution and their ability to directly visualize enzymatic conversion of glutamine to glutamate. Recent developments in the field of hyperpolarized magnetic resonance have provided methods to assess enzymatic flux (19, 20) and to develop strategies to hyperpolarize glutamine (21–25). Previous attempts to leverage

Author contributions: K.R.K. designed research; R.E., N.K., A.M., M.S., M.B., and A.J.P. performed research; K.L.G. contributed new reagents/analytic tools; R.E., N.K., G.Z., and J.C. analyzed data; and R.E., N.K., J.C., C.B.T., and K.R.K. wrote the paper.

Reviewers: N.C., Northwestern University; and J.S., University of California, Davis.

Competing interest statement: C.B.T. is a founder of Agios Pharmaceuticals and a member of its scientific advisory board. K.R.K. is a member of the scientific advisory boards of NVision Imaging Technologies and Imaginoistics. C.B.T. and K.R.K. are inventors on patent applications related to imaging cellular metabolism.



[1]To whom correspondence may be addressed. Email: rahimikk@mskcc.org or ThompsonC@mskcc.org.

This article contains supporting information online at http://www.pnas.org/lookup/suppl/doi:10.1073/pnas.2120595119/-/DCSupplemental.

Published May 5, 2022.

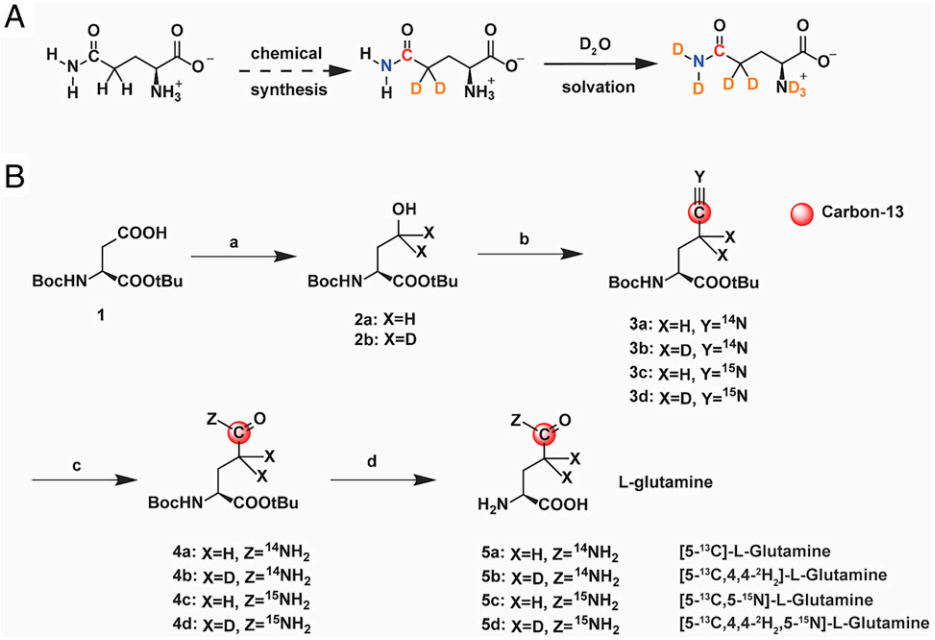


**Fig. 1.** Synthetic scheme for site-specific isotope labeling of glutamine. (*A*) Schematic for generation of hyperpolarized glutamine to detect in vivo metabolic flux. (*B*) (*a i*) ClCOOEt, $NEt_3$, THF, −5 °C, 30 min. (*ii*) $NaBD_4$, $D_2O$, 0 °C, 1 h. (*b*) [$^{13}C$,$^{15}N$]-KCN,18-Crown-6, P(n-Bu)$_3$, $CCl_4$, $CH_3CN$, room temperature (rt), 24 h. (*c*) acetaldoxime, $RhCl(PPh_3)_3$ (0.5 mol%), toluene, 110 °C, 24 h. (*d*) TFA/DCM (1:1), rt, 12 h.

this platform have been complicated by side reactions, low substrate solubility, and incomplete transfer of polarization, thus making in vivo assessment of glutaminase flux challenging.

Glutaminase is an aminohydrolase enzyme that converts the glutamine amide group to a carboxylate in glutamate. Prior hyperpolarized studies using [5-$^{13}$C]-L-glutamine confirmed that detecting the carbon-5 resonance of [5-$^{13}$C]-L-glutamate with $^{13}$C NMR could be used to monitor glutaminase reaction dynamics in vitro. However, the presence of $^{14}$N dramatically reduces the signal persistence outside the polarizer, due to quadrupolar-mediated scalar relaxation at low magnetic fields (26). At high magnetic fields, $^{14}$N also results in increased linewidth and thus limits the signal-to-noise ratio (SNR) achievable for glutamine in vivo. Furthermore, previous preparations generated significant amounts of labeled pyroglutamate, a cyclic side product that overlaps with [5-$^{13}$C]-L-glutamate and obscures the ability to visualize metabolic flux in vivo.

In this work, we provide a modular synthetic strategy for $^{13}$C, $^{2}$H(D), $^{15}$N isotope-labeled glutamine. Our strategy results in high yields, and enriching with deuterium next to the side chain carbonyl (at carbon 4) provides an increase in $T_1$ relaxation time through decreased long-range dipolar relaxation. In addition, $^{15}$N-labeling decreases low field quadrupolar relaxation, resulting in both increased polarization and longer $T_2$ relaxation time. Using this labeling strategy, in combination with an optimized preparation, we overcome many of the limitations of previous approaches. Additionally, we observed greatly reduced hyperpolarized signals arising from the chemical side-product pyroglutamate due to the presence of an adjacent $^{14}$N, which only occurs in the cyclized molecule. Given the relevance of glutaminase flux in pancreatic ductal adenocarcinoma (PDAC) (27, 28), we leveraged this approach to measure in vivo enzyme kinetics in models of PDAC with treatment using a glutaminase inhibitor and confirmed these results using stable-isotope tracing mass spectrometry. Taken together, our results demonstrate a systematic study of a hyperpolarized glutamine probe with multiple stable-isotope enrichments that overcomes many of the limitations encountered in previous attempts to assess glutamine flux and thereby provides a window into this key metabolic pathway in vivo.

## Results

**Synthesis of C5 Hyperpolarized Glutamine Probes with Multiple Stable-Isotope Enrichments.** To resolve glutamine from its GLS-mediated product glutamate using hyperpolarized magnetic resonance, a significant chemical shift difference is required as well as a long spin-lattice relaxation time ($T_1$) to facilitate probe delivery and conversion in a biologically relevant time frame. Previous work has identified the carbon-1 (C1) of glutamine as a long $T_1$ nucleus, but glutamine could not be resolved from glutamate in vivo due to an inadequate chemical shift difference (24). While the carbon-5 (C5) position provides a larger chemical shift difference, visualization of in vivo flux through GLS has been unattainable due to short $T_1$ at low magnetic fields, short spin-spin relaxation ($T_2$) at high magnetic fields, and spectral overlap of byproducts.

Building on previous work (29), we have developed a multistep synthesis for isotopically enriching the C5 position of glutamine, incorporating $^{2}$H and $^{15}$N, using commercially available precursors (Fig. 1 and *SI Appendix*, *Supplementary Methods*). Using this approach, we synthesized all relevant combinations of isotopes about the C5 position to explore the benefit of selective enrichment. Measuring at 14.1 T (Fig. 2*A*), the glutamine C5 resonance $T_1$ increased with $^{2}$H-enrichment ~18% ([5-$^{13}$C]-L-glutamine $T_1$ = 10.8 ± 0.55 s and [5-$^{13}$C,4,4-$^{2}$H$_2$]-L-glutamine $T_1$ = 12.74 ± 0.69 s), while $^{15}$N-enrichment provided minimal increase at high field ([5-$^{13}$C,5-$^{15}$N]-L-glutamine $T_1$ = 10.9 ± 0.5 s). Triple-labeling ([5-$^{13}$C,4,4-$^{2}$H$_2$,5-$^{15}$N]-L-glutamine) did not further increase the $T_1$ significantly over just $^{2}$H enrichment.

As most of the applications of hyperpolarized magnetic resonance are conducted at lower magnetic fields where $T_1$ is longer due to reduced chemical shift anisotropy-mediated relaxation, we explored the $T_1$ relaxation times of these molecules at 1.0 T. Molecules were hyperpolarized using dissolution

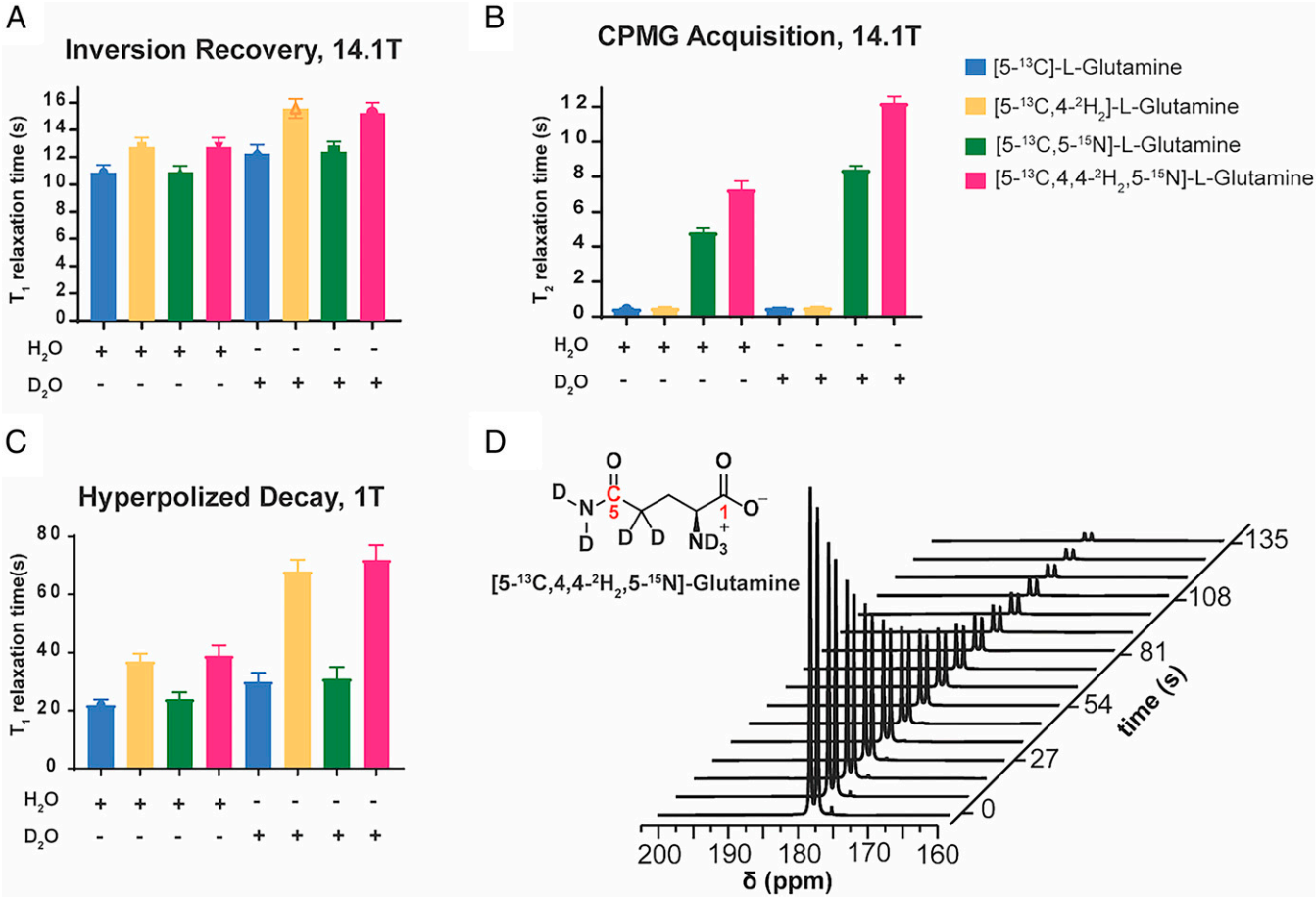


**Fig. 2.** Relaxation times are longer for glutamine with multienrichment with elimination of side product contaminants. (*A*) $T_1$ relaxation times for four different labeling patterns of 30 mM glutamine C5 resonance measured at 14.1 T in $H_2O$ or $D_2O$, 200 mM phosphate at pH 7.4. (*B*) $T_2$ relaxation time of the C5 resonance measured at 14.1 T for four different labeling patterns of 30 mM glutamine C5 resonance measured at 14.1 T in $H_2O$ or $D_2O$, 200 mM phosphate at pH 7.4. (*C*) Hyperpolarization decay of four different labeling patterns of glutamine C5 resonance measured at 1.0 T in $H_2O$ or $D_2O$. (*D*) Hyperpolarization decay of [5-$^{13}$C,4,4-$^{2}$H$_2$,5-$^{15}$N]-L-glutamine in 200 mM phosphate buffer in $D_2O$ acquired with a 10° excitation every 3 s (every third spectra is shown). All measurements were made in triplicate and are reported as mean ± SD and acquired at standard temperature and pressure (STP).

dynamic nuclear polarization, and their decay demonstrated a dramatic increase in $T_1$ relaxation time with the [5-$^{13}$C,4,4-$^{2}$H$_2$,5-$^{15}$N]-L-glutamine relaxation in phosphate buffer in $D_2O$ ~3.3-fold higher ($T_1$ = 72 ± 5 s, Fig. 2*C*). Given that clinical translation of these biochemical probes drives their development, we further characterized the lifetime of [5-$^{13}$C,4,4-$^{2}$H$_2$,5-$^{15}$N]-L-glutamine at 3 T finding it to be 62.4 ± 2.4 s, well within the range of translation.

Previous attempts to image glutamine conversion to glutamate were confounded by the generation of side products that overlap with the C5 glutamate resonance, especially pyroglutamate. These byproducts are typically detected on the order of the natural abundance signal of the C1 glutamine (21, 25, 30). Standard approaches, including freezing of glutamine in high concentrations of NaOH during polarization, are unable to mitigate the formation of pyroglutamate. However, by utilizing a slightly acidic phosphate buffer to account for the NaOH in the dissolution, we obtained a neutral solution with no side production of pyroglutamate or glutamate, as highlighted in the hyperpolarized $^{13}$C dynamic decay (Fig. 2*D*). This is a result of the cyclization mechanism of pyroglutamate formation, which brings the $^{14}$N-alpha amine in proximity to the C5 of glutamine (*SI Appendix*, Fig. S1). While this is not detrimental at high-fields, quadrupolar-mediated relaxation at low fields (e.g., <0.05 T) is efficient at reducing hyperpolarized signal, and during dissolution, this effectively eliminates any detectable pyroglutamate. Taken together, these methods provide a solution to overcoming previous limitations of this system.

**Spatially Resolved Hyperpolarized Glutamine MRSI Quantitatively Assesses Glutamate Formation.** To confirm that hyperpolarized (HP) [5-$^{13}$C,4,4-$^{2}$H$_2$,5-$^{15}$N]-L-glutamine can be used to characterize tumors in vivo, we acquired spatially resolved MRSI data following injection of HP glutamine. $^{13}$C spectra from regions of tumor as well as the normal adjacent kidney demonstrate rapid conversion of HP glutamine to glutamate (Fig. 3*B*). While more HP glutamine reaches the adjacent kidneys, it is clear that tumors are more glutaminolytic, producing more HP glutamate relative to the glutamine which reaches the tumor (Fig. 3*C*). This is further exemplified in ratio maps (Fig. 3*E*) and consistent across mice when normalized to a 4.0 M $^{13}$C urea standard placed in the field of view (Fig. 3 *F* and *G*) as well as in ratios of HP glutamate/glutamine (Fig. 3*H*).

**HP [5-$^{13}$C,4,4-$^{2}$H$_2$,5-$^{15}$N]-L-Glutamine Magnetic Resonance Measures Flux to Glutamate In Vivo.** To demonstrate the utility of HP [5-$^{13}$C,4,4-$^{2}$H$_2$,5-$^{15}$N]-L-glutamine in monitoring glutamine metabolism in vivo, we utilized pancreatic cancer xenograft models which are known to be glutamine avid (27) and, to verify that the conversion via glutaminase was on target, we leveraged the well-characterized glutaminase inhibitor, CB-839. In these experiments, MIA PaCa-2 xenografts were implanted

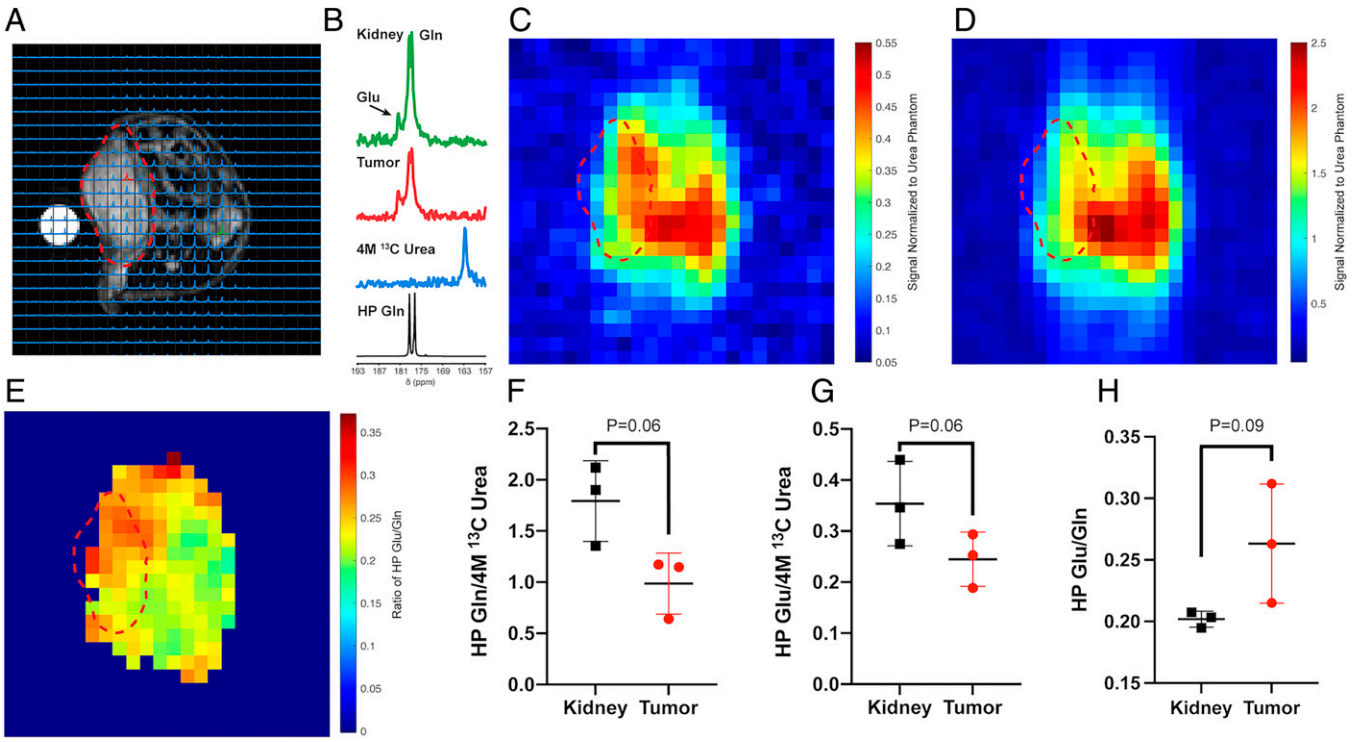


**Fig. 3.** Spatially resolved HP glutamine to glutamate conversion allows for in vivo quantitation of glutaminolysis in a murine pancreatic cancer model. (*A*) Anatomic $T_2$-weighted MRI with $^{13}C$ overlay. The MIA PaCa-2 tumor region is highlighted with a red dotted line. (*B*) Representative $^{13}C$ spectra from the tumor and contralateral kidney as well as adjacent 4.0 M $^{13}C$ urea phantom and dissolution media (*Bottom*) are shown postinjection of HP [5-$^{13}C$,4,4-$^{2}H_2$,5-$^{15}N$]-L-glutamine. (*C* and *D*) HP glutamate (*C*) and HP glutamine (*D*) images were calculated from integrating the peak in each voxel and demonstrate in vivo conversion of the probe to its product. (*E*) Ratio map of HP Glu/Gln demonstrates increased conversion in the tumor. (*F–H*) Quantified data for normalized HP glutamine, glutamate, and the Glu/Gln ratio across tumors ($n$ = 3 per group). An increased conversion ratio is observed in regions of tumor. All data are reported as the mean ± SD and listed $P$ values from Student's $t$ test.

subcutaneously, and mice were imaged 2 h after administration of vehicle or CB-839 (single dose, 200 mg/kg oral gavage) (Fig. 4*A*). We had previously validated this was an appropriate drug concentration in a separate cohort of tumor-bearing mice by measuring CB-839 concentration over time using liquid chromatography-mass spectrometry (LC-MS). These experiments determined that >1 nmol/g CB-839 could be detected in tumor tissue 2 h post oral gavage with 200 mg/kg (Fig. 4*B*), in agreement with previous studies in pancreatic cancer models (31). Sagittal slab dynamic $^{13}C$ HP MRS in a mouse injected with hyperpolarized [5-$^{13}C$,4,4-$^{2}H_2$,5-$^{15}N$]-L-glutamine revealed in vivo conversion to hyperpolarized glutamate (Fig. 4*C*). Treatment with CB-839 dramatically reduced conversion to glutamate both in the ratio of glutamate to glutamine (Fig. 4*D*) and the unidirectional rate constant derived from the dynamic data (Fig. 4*E*). While rapid generation of [$^{13}C_5$]glutamate is observed in tumors, treatment with CB-839 prior to infusion resulted in a significant decrease in [$^{13}C_5$]glutamate production ($P < 0.01$) (Fig. 4 *F* and *G*). This change in glutamate labeling is not due to differential availability of labeled glutamine in the tumor (*SI Appendix*, Fig. S2*A*). These results were further validated using stable-isotope tracing following tail-vein injection of [$^{13}C_5$]glutamine and analysis of tumor extracts by LC-MS at 2, 5, and 10 min postinfusion (Fig. 4*G* and *SI Appendix*, Fig. S2 *B–D*). Interestingly, a reduction in the labeling of other key TCA cycle intermediates, including m+4 citrate, m+4 succinate, m+4 malate, and m+4 aspartate is also observed with glutaminase inhibition (Fig. 4 *H–K*), highlighting the role of glutaminase in feeding the carbon backbone of the TCA cycle in the mitochondria. Taken together, these rapid isotope tracing data support the quantitative decrease in flux observed noninvasively in the hyperpolarized glutamine MRS experiment.

## Discussion

In this work, we report a high-yield, multistep synthesis for [5-$^{13}C$,4,4-$^{2}H_2$,5-$^{15}N$]-L-glutamine from commercially available precursors. Although [5-$^{13}C$]-L-glutamine is commercially available, nuclear spin-spin coupling between carbon-4 protons and carbon-5 is observed as a triplet in $^{13}C$-NMR in the absence of $^{1}H$-decoupling, suggesting that the carbon-4 protons have the potential to exhibit significant dipole-dipole relaxation on carbon-5. Our results demonstrate that deuteration at the carbon-4 position yields longer carbon-5 relaxation times, supporting the advantage of reducing this relaxation pathway. Previous work has proposed that deuteration at the carbon-4 position could be beneficial for hyperpolarized glutamine detection (32), however it is clear from that work that the resulting polarization and $T_1$ were still limiting, precluding that approach from being used in vivo. In addition, $^{14}N$-nuclei covalently bound to carbon-5 act as sites of scalar relaxation, which shortens both $T_1$ and $T_2$ relaxation times. This relaxation is further extended with $^{15}N$-enrichment at this directly bonded nitrogen resulting in improved SNR and spectral resolution due to decreased scalar relaxation. Previous studies have explored the use of [$^{13}C$,$^{15}N$]urea to achieve increased imaging resolution, arguing that a lengthening of $^{13}C$ $T_2$ can facilitate enhanced spatial resolution (33). This work highlights the advantages of $^{15}N$-enrichment for HP probes with $^{13}C$-enrichment on amide-like functionalities as a generalized approach for hyperpolarization, and similar benefits should be achieved when this is

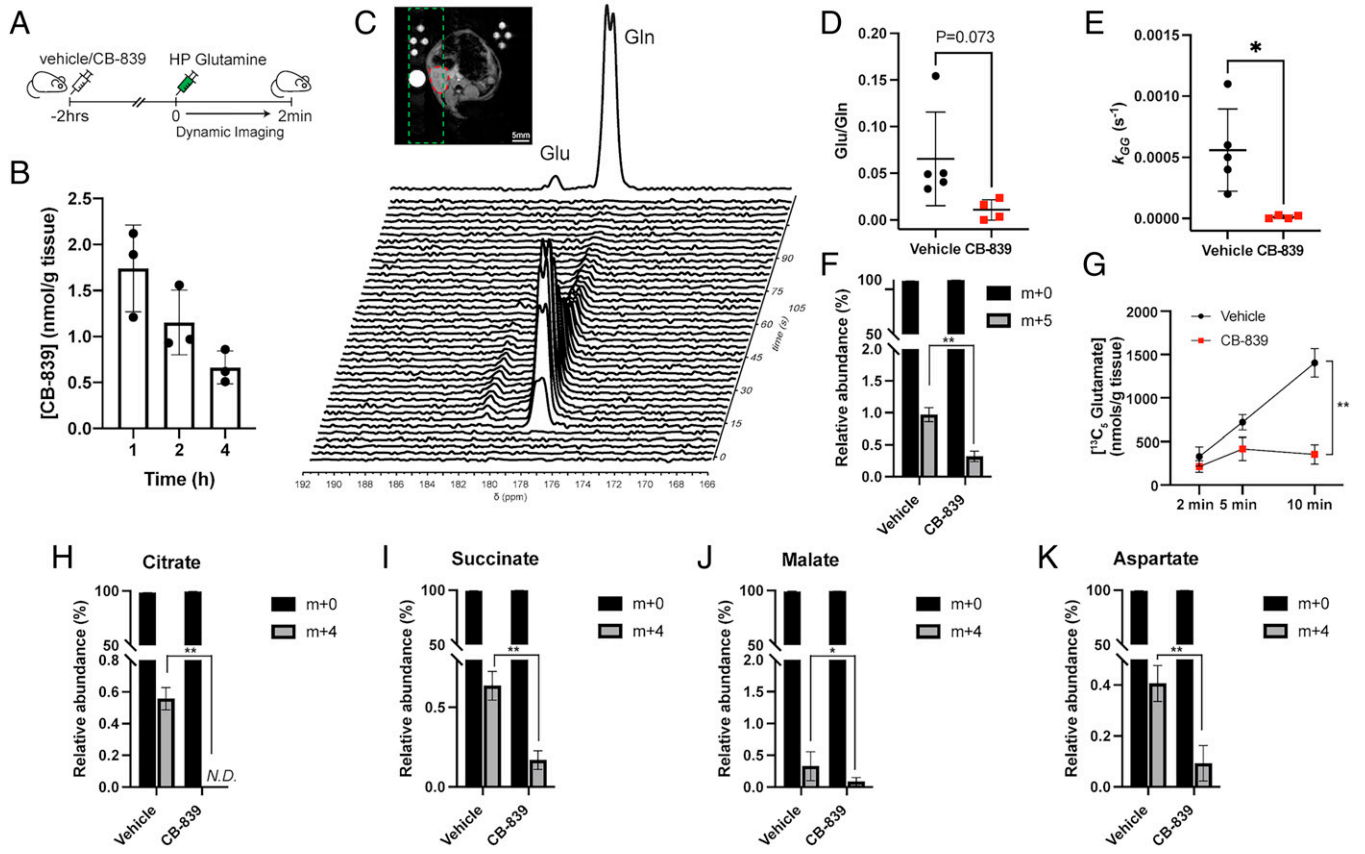


**Fig. 4.** Conversion of HP glutamine to glutamate can be quantified and inhibited using a glutaminase inhibitor (GSLi). (*A*) Scheme for treatment and imaging with HP [5-$^{13}$C,4,4-$^{2}H_2$,5-$^{15}$N]-L-glutamine. (*B*) LC-MS confirmation of delivery of the GLSi CB-839 to MIA PaCa-2 tumors. (*C*) *Top*: Representative $T_2$-weighted MRI and the localization of the slab excited for $^{13}$C dynamic MRS. *Bottom*: Representative $^{13}$C MRS spectra demonstrating probe delivery in vivo and subsequent conversion with a single time point at 30 s shown above for clarity. (*D*) Quantification of the glutamate to glutamine AUC ratio (Glu/Gln) for all time points following treatment with CB-839. The ratio decreases with treatment, approaching significance, $P = 0.073$. (*E*) Flux rate for conversion of glutamine to glutamate ($k_{GG}$), with the flux significantly decreasing following treatment with CB-839. (*F*) Relative abundance of m+0 and m+5 glutamate 10 min after injection of [$^{13}C_5$]glutamine in MIA PaCa-2 tumor-bearing mice following treatment with CB-839. (*G*) Quantitation of [$^{13}C_5$] glutamate at time points after injection of [$^{13}C_5$]glutamine demonstrating significant reduction in flux to glutamate following treatment with CB-839. (*H–K*) Relative abundance of the m+0 and m+4 isotopomers of key TCA cycle intermediates 10 min after injection of [$^{13}C_5$]glutamine in MIA PaCa-2 tumor-bearing mice following treatment with CB-839. $^*P < 0.05$, $^{**}P < 0.01$. All data reported as mean ± SD. not detected (N.D.).

applied to other probes with this functional group, such as thioureas (34), small peptides (35), and amino acid derivatives (19, 36).

This work represents a demonstration of noninvasive, in vivo detection of glutamine metabolism through glutaminase without overlap of contaminating resonances, in part facilitated by the improved spectral properties afforded by $^{2}H$ and $^{15}N$-enrichments. We confirmed the flux decrease observed by HP MRI in vivo using [$^{13}C_5$]glutamine isotope tracing and LC/MS analysis of xenograft tumor extracts within 10 min of infusion. While technically challenging due to strong signal suppression by the large preexisting unlabeled glutamate pool, this validation in vivo provided a means of truly assessing the decrease in glutamate production with rapid glutaminase inhibition and validates our probe is on target. By HP glutamine flux measurements, we derive a rate of ∼0.03 $min^{-1}$ and confirm a rate of 150 nmol/min/g by rapid isotope tracing in vivo which is well in line with contemporary work using isotope tracing in flank PDAC tumors (37).

Biologically, our work shows in vivo the importance of glutaminase to convert glutamine into fueling the carbon intermediates of the TCA cycle in the mitochondria. This confirms in vitro studies suggesting tumor cell lines engage in glutaminolysis to sustain TCA cycle anaplerosis. In future studies, it will be of great interest to study the role of oncogenic mutations, like c-*Myc*, in driving glutaminolysis and the extent to which glutamine is further partitioned in the cell to support nucleotide biosynthesis as opposed to the TCA cycle (8, 38). Mutations in *KRAS* and loss of *p53* have been implicated as drivers of pancreatic cancer and play a critical role in glutaminolysis (27, 39, 40). This work provides a further basis to explore these drivers in vivo. Here, using glutaminase modulation in combination with HP glutamine, we demonstrate clear evidence of a dramatic decrease in glutamine flux linked to the TCA cycle as seen in the lack of generation of m+4-labeled citrate following treatment with CB-839 in the context of rapid [$^{13}C_5$]glutamine administration in pancreatic cancer models. We show that HP glutamine MRS provides a means of determining the extent of glutamine amine donation to the cell through the TCA cycle noninvasively.

Given the recent interest in unraveling the importance of glutaminase activity in various tumor types and the mixed results of clinical trials with glutaminase inhibitors, hyperpolarized [5-$^{13}$C,4,4-$^{2}H_2$,5-$^{15}$N]-L-glutamine can be used as a tool to advance this research as well as aid in drug development. In addition, given the efficient translation of hyperpolarized probes into humans to characterize cancer biology (20, 39–42), this imaging approach is readily clinically translatable and it is possible that hyperpolarized [5-$^{13}$C,4,4-$^{2}H_2$,5-$^{15}$N]-L-glutamine can be used to image glutamine metabolism in humans in the future. Multiple clinical trials are underway to target

glutaminase in patients with a wide range of cancers (43, 44), this imaging biomarker could unlock the ability to assess on-target inhibition in vivo and guide future trials.

As a future direction for this work, we intend to take advantage of the long carbon-5 $T_2$ and explore the use of longer echo-train acquisitions with increased imaging resolution. The use of a $^{2}H$ and $^{15}N$-decoupler will further unlock the potential of this probe, as it will collapse the carbon-5 doublet to a singlet, increasing SNR by a factor of ∼2 and improving spectral resolution. Glutamine variants with different heavy-atom labeling schemes, as well as other amino acids, can be synthesized by implementing minor changes to the scheme in Fig. 1*B* due to the modular nature of our synthetic route.

Applications of [5-$^{13}$C,4,4-$^{2}H_2$,5-$^{15}$N]-L-glutamine are also not just limited to hyperpolarized $^{13}$C-NMR or MRI. Since $^{2}H$ itself is detectable by magnetic resonance approaches, this molecule may be used to assay glutaminase flux via using thermal-equilibrium NMR. [5-$^{13}$C,4,4-$^{2}H_2$,5-$^{15}$N]-L-glutamine can be injected intravenously or added to tissue culture media, and $^{2}H$-NMR of tissue extracts, cell extracts, or cell media can be performed to follow the metabolic fates of glutamine. Aside from MR applications, this approach can also be used for mass-spectrometry-based metabolic tracing studies via detection of $^{13}C$-, $^{2}H$-, and $^{15}N$-enrichment in downstream metabolites. This can be applied to metabolomic profiling of cell culture or tissue extracts (45) from animals injected with [5-$^{13}$C,4,4-$^{2}H_2$, 5-$^{15}$N]-L-glutamine, as well as ex vivo metabolite imaging of tissue slices or cells using desorption electrospray ionization (46) imaging or multi-isotope imaging mass spectrometry (47) with higher spatial resolution. In theory, this logic may be employed to follow glutamine uptake along with ion-beam analysis but this has yet to be demonstrated.

Overall, this work highlights the potential of [5-$^{13}$C,4,4-$^{2}H_2$,5-$^{15}$N]-L-glutamine as an in vivo hyperpolarized imaging probe, with the ability to quantitatively determine the extent of glutamine metabolism in the mitochondria, and future experiments will be designed toward further exploring the utility of this molecule.

## Materials and Methods

**Cell Lines and Culture Conditions.** MIA PaCa-2 (male) human pancreatic cancer cells were cultured and maintained in Dulbecco's modified Eagle's medium supplemented with 10% fetal bovine serum, and 100 mg/mL streptomycin prepared at Memorial Sloan Kettering Media Preparation core and grown as monolayers at 37 °C with 5% $CO_2$. Cell lines were validated at the Integrated Genomics Operation core at Memorial Sloan Kettering Cancer Center.

**Mice.** All animal experiments were approved by the Institutional Animal Care and Use Committee at Memorial Sloan Kettering Cancer Center. Female athymic nude mice (4- to 6-wk-old, average weight 25 g, Jackson Laboratories) were xenografted on the right flank via subcutaneous injection of $5.0 \times 10^{6}$ cells. Cells were injected in a 150 mL suspension of 1:1 V/V PBS with Matrigel. All mice were housed under standard conditions (group housing up to five per cage) with ad libitum access to food and water and 12 h light/dark cycle. Tumors were allowed to develop until a size of 0.25 to 0.35 cc for HP-MRI experiments and LC-MS analysis.

**Synthesis of Isotope-Enriched Glutamine Probes.** The synthetic scheme for glutamine probes is demonstrated in Fig. 1 and was modified from previously published work on similar compounds. Each reaction of the multistep synthesis was optimized to give an overall yield of 50% for glutamine (*SI Appendix, Supplementary Methods* include each intermediate). The final product was purified via by recrystallization. Reaction conditions for each step are listed in *SI Appendix*.

**$T_1$ and $T_2$ Measurement at High Field (14.1 T).** A 14.1 T NMR spectrometer (Bruker BioSpin) was used to measure thermal-equilibrium $T_1$ and $T_2$ relaxation times of the carbon-5 resonance of the variants of isotopically enriched glutamine. As previously described (29), in separate NMR tubes, each compound was dissolved to a final concentration of 30 mM in $D_2O$ solution or 1:19 solution of $D_2O$:$H_2O$ and 100 mM Tris, and 1.0 mM EDTA and final pH adjusted to 7.4 $D_2O$ was added to the mixture to facilitate spin-locking to minimize $B_0$ drift. Thermal-equilibrium $T_1$ was measure using a standard inversion-recovery sequence with 16 averages and delay times ranging from 1 s to 45 s between the 180° and 90° pulses. Thermal-equilibrium $T_2$ values were measured using a Carr-Purcell-Meiboom-Gill sequence on the same samples. Echo times ($\tau$) between 0.01 and 100 s were sampled. A 100 s ($>5 \times T_1$) wait time was implemented between scans to allow sufficient time for full longitudinal recovery. For both $T_1$ and $T_2$ measurements, the area under the curve (AUC) of the carbon-5 resonance was integrated using Mnova (Mestrelabs) and AUC values were exported to Prism 8 (GraphPad Software) for curve fitting. AUC vs. time was fit to a mono exponential function, and $T_1$ and $T_2$ values were reported with a 95% confidence interval.

**Hyperpolarization of [5-$^{13}$C,4,4-$^{2}H_2$,5-$^{15}$N]-L-Glutamine.** Due to reported instability of the basic glutamine prep, fresh preparations were used for each experiment made from 20 mg of [5-$^{13}$C,4,4-$^{2}H_2$,5-$^{15}$N]-L-glutamine in 14 μL NaOH (10 N), then mixed with 13.0 mg of a mixture of 8.2% OX063 (Oxford Chemicals) in glycerol. The final concentration of glutamine was 4 M and OX063 was 15 mM. The sample was sonicated in ice-chilled water for 10 min and subsequently polarized with dynamic nuclear polarization in a SPINlab Polarizer (General Electric) for over 2 h (5.0 T, 0.80 K, 139.995 GHz). Following polarization, the HP substrate was removed from the polarizer via rapid dissolution, during which the hyperpolarized sample was dissolved in a superheated aqueous solution of 200 mM phosphate buffer in $H_2O$ or $D_2O$, 0.1 mM EDTA, pH 2.5, and collected into a vial at room temperature and directly used for further experiments.

**Polarization Level, Apparent Hyperpolarized $T_1$.** All 1.0 T measurements were acquired on a SpinSolve 1.0 T NMR spectrometer (Magritek) and all 3 T measurements were made using a 3 T MRI equipped with a dual-tuned $^{1}H/^{13}C$ coil (Bruker BioSpin). For hyperpolarized $T_1$ measurements, 700 μL of the HP dissolution was loaded in the spectrometer ∼30 s postdissolution, and spectra were acquired every 5 s with 5° excitations, analogous to previously described experiments (29). The AUC of the resonance of interest as a function of time was fit to the solution of the Bloch equation for $T_1$, including polarization loss from each excitation. $^{13}C$ polarization levels were calculated by comparing the carbon-5 AUC from the first HP spectrum with thermal-equilibrium carbon-5 AUC of the same sample. For thermal-equilibrium measurements, the HP sample was allowed to depolarize to thermal-equilibrium polarization, after which a solution of 0.5 M Gd-DOTA in $H_2O$ was added to a final concertation of 1.0 mM. A $^{13}C$-NMR spectrum was subsequently acquired using a 1.0-T spectrometer with a 90° excitation, 10-s repetition time, and 8192 averages. Polarization levels were calculated by multiplying the $^{13}C$ polarization levels at 1.0 T and 300 K (calculated as 0.000086% based on the Boltzmann distribution) by the ratio of the HP signal to the thermal-equilibrium signal, (corrected for differences in excitation angle and number of averages between the two measurements) and extrapolating back to the time of dissolution using the measured hyperpolarized $T_1$ at 1.0 T.

**1D and 2D HP Glutamine MRSI Acquisition and Data Processing.** All imaging experiments were conducted using a Bruker 3 T MRI equipped with a dual-tuned $^{1}H/^{13}C$ coil (Bruker BioSpin). For each experiment a female nude (4 mo; Jackson Laboratories) was cannulated with a 23-gauge rodent tail-vein catheter (Braintree Scientific). The catheter was prefilled with 10 U heparin/mL in normal saline to keep the mouse heparinized prior to injection with the hyperpolarized substrate, and the mouse was anesthetized using a continuous flow of 1 L/min oxygen with 1.5% isoflurane. Mice were restrained in a plastic Mouse DecapiCone Restrainer (Braintree Scientific) on the MRI bed, which was equipped with a warm-water blanket and nose cone for oxygen/isoflurane delivery, and a 4.0 M $^{13}C$-urea phantom was placed underneath the mouse. The mouse was subsequently loaded inside the coil and centered about its abdomen. Axial anatomic $T_1$-weighted images were acquired with $0.313 \times 0.313$ $mm^2$ resolution across 12 slices throughout the mouse abdomen, and the

radiofrequency power for $^{13}C$ excitation was calibrated using the $^{13}C$-urea phantom. The magnetic field was shimmed throughout a 15-mm slab containing the mouse liver and kidneys, the same region used for hyperpolarized [5-$^{13}C$,4,4-$^{2}H_2$,5-$^{15}N$]-L-glutamine imaging experiments. One minute before the start of the imaging experiment, the oxygen/isoflurane was set to 0.4 L/min with 0.25% isoflurane. 1 min before dissolution, isoflurane was turned off to let the mouse wake up. Following dissolution of hyperpolarized [5-$^{13}C$,4,4-$^{2}H_2$,5-$^{15}N$]-L-glutamine, the mouse was injected with 250 μL of the dissolution over 10 s through the tail-vein catheter. Note that this injected volume excludes the 100 μL of 10U heparin/mL solution in the dead volume of the catheter.

***For 1D slab dynamic experiments.*** Immediately following the end of the injection, a series of $^{13}C$ spectra were collected across the preshimmed 15-mm slab with a 3-s repetition time and a 30° excitation. Data were processed using standard methods as previously described (29). Experimental signal integrals in the hyperpolarized $^{13}C$ experiments, $M_{z,glutamine}$ and $M_{z,glutamate}$, were quantitatively modeled using the following equations:

$$\frac{dM_{z,glutamine}(t)}{dt} = -k_{glutamine-glutamate} \times M_{z,glutamine}(t) - (R_{1,glx} + \lambda) \times M_{z,glutamine}(t)$$
$$\frac{dM_{z,glutamate}(t)}{dt} = k_{glutamine-glutamate} \times M_{z,glutamine}(t) - (R_{1,glx} + \lambda) \times M_{z,glutamate}(t)$$

where $k_{glutamine-glutamate}$ is the observed rate constant for the conversion from glutamine to glutamate, $R_{1,glx}$ is the longitudinal relaxation rate of carbon-5, and assumed to be the same for both glutamine and glutamate, and $\lambda = \ln(\cos(\alpha))/\Delta t$, with $\alpha = 30^o$ and $\Delta t = 3s$, accounts for signal depletion due to the excitation pulses (48). The fitting was conducted using MATLAB (The MathWorks). For each dataset, the signal integrals were normalized to the maximum value. A nonlinear least-squares method was used to obtain the fitting parameters, $k_{glutamine-glutamate}$ and $R_{1,glx}$.

***2D MRSI experiments.*** Twenty seconds after the end of injection, $^{13}C$ MR data were acquired using an axial 2D CSI sequence with a 20° excitation, 12 × 12 matrix, 40 × 40 $mm^2$ field of view (FOV), and 10-mm slice thickness. For each spectrum, a total of 384 complex points were acquired with a total acquisition time of 10.1 s. Data were processed as previously described for HP glutamine (24). Briefly, the data were zerofilled, apodized, and Fourier transformed using MATLAB. Peaks for glutamine and glutamate were identified and the total area of each peak was integrated to produce maps of each metabolite. Additionally, a 4.0 M $^{13}C$ urea standard was placed in the FOV and used for data normalization. Integrals of glutamine and glutamate were normalized to the signal from the urea standard and corrected for polarization level measured on the dissolution sample. Regions of interest were defined using $T_2$-weighted $^{1}H$ MRI data acquired with the same FOV to measure average glutamine, average glutamate, and the ratio of glutamate/glutamine (Glu/Gln) in the tumors and contralateral kidney.

**LC-MS Analysis in Tumor Tissues.** Tumor-bearing animals were restrained and kept under isoflurane flow. A 300 μL bolus of buffered [$^{13}C_5$]glutamine (30 mM in Tris) was intravenously injected (over 12 s) into lateral tail vein of MIA PaCa-2 tumor-bearing mice. Animals were euthanized 2 min, 5 min, and 10 min after the start of injection for Gln infusions. Tumors were quickly resected and snap frozen in liquid nitrogen. Tumor tissues were ground in a cooled mortar and pestle with liquid nitrogen, and ∼30 mg of powdered tissue was weighed in a 2-mL prefilled bead tube (2.8-mm ceramic beads, OMNI International). The powdered tissue was extracted using 4:4:2 acetonitrile:methanol:water to a final tissue concentration of 50 mg/mL and further homogenized in a Biotage Bead Ruptor 24 (3 cycles of 30 s) at 4 °C. Thereafter, samples were centrifuged at 20,000 × *g* for 20 min at 4 °C, and 300 μL of supernatant was collected and dried in a vacuum concentrator (Genevac EZ-2 Elite, The Lab World Group) for 3 h. For [$^{13}C_5$]glutamate quantification, dried tissue extracts were resuspended in 50 μL of 97:3 water:methanol containing 10 mM tributylamine and 15 mM acetic acid. For profiling of other TCA cycle intermediates, extracts were resuspended in 100 μL of 50:50 water:methanol. After resuspension in the respective volumes, samples were vortexed, incubated on ice for 20 min, and centrifuged at 20,000 × *g* for 20 min at 4 °C.

Quantification of GLSi (CB-839) was performed using an Agilent 6550 Q-TOF mass spectrometer in positive ionization mode, coupled to a BEH X-Bridge C-18 column (150 mm × 2.1 mm, 3.5 μm particle size, Waters). Mobile Phase A consisted of 10 mM ammonium bicarbonate in water and Mobile Phase B consisted of 10 mM ammonium bicarbonate in 90:10 methanol:water. LC gradient conditions were: 0 min at 0% B, 1.5 min at 0% B; and 18 min at 100% B. Other LC parameters were: flow rate at 0.4 mL/min, column temperature 45 °C, and injection volume was 5 μL. MS source parameters included: gas temp, 240 °C; gas flow, 18 L/min; nebulizer pressure, 25 psig; sheath gas temp, 400 °C; sheath gas flow, 10 L/min; VCap, 4000 V; nozzle voltage, 0 V; and fragmentor, 175 V. Calibration curves were prepared using a 10 mM stock of CB-839 in dimethylsulfoxide (DMSO) and data analysis was performed using Agilent MassHunter Profinder 10.0.

Quantification of [$^{13}C_5$]glutamate was performed using an Agilent 6470 triple quadrupole mass spectrometer operating in negative ionization mode, coupled to a ZORBAX Rapid Resolution High Definition Extend C-18 column (150 mm × 2.1 mm, 1.8 μm particle size, Agilent). Mobile Phase A consisted of 10 mM tributylamine and 15 mM acetic acid in 97:3 water:methanol, and Mobile Phase B consisted of 10 mM tributylamine and 15 mM acetic acid in methanol. LC gradient conditions were: 0 min at 0% B; 7.5 min at 20% B; 13 min at 45% B; 20 min at 99% B; and 24 min at 99% B. Other LC parameters were: flow rate at 0.25 mL/min, column temperature 35 °C, and injection volume was 5 μL. MS source parameters included: gas temp, 150 °C; gas flow, 13 L/min; nebulizer pressure, 45 psig; sheath gas temp, 325 °C; sheath gas flow, 12 L/min; VCap, 2000 V; and nozzle voltage, 500 V. MRM transitions and collision energies (CE) were as follows: [$^{13}C_5$]glutamate *m/z* 151.1 → 106.0 (CE: 12V)*; 133.0 (CE: 8V) with * indicating the primary transition used for quantification. Calibration curves were prepared using [$^{13}C_5$]glutamate spiked in tumor tissue extract from untreated mice to correct for ion suppression due to high concentration of unlabeled glutamate present in the extracts. Data analysis was performed using Agilent MassHunter Quantitative Analysis 10.1 for QQQ (Agilent Technologies).

Metabolite profiling of TCA cycle intermediates was performed using an Agilent 6230 time-of-flight mass spectrometer under negative ionization coupled to an Xselect HSS T3 column (150 mm × 2.1 mm, 3.5 μm particle size, Waters). Mobile Phase A consisted of 5 mM octylamine and 5 mM acetic acid in water, and Mobile Phase B consisted of 5 mM octylamine and 5 mM acetic acid in methanol. LC gradient conditions were the following: 0 min at 1% B; 3.5 min at 1% B; 4 min at 35% B; 15 min at 35% B; 20 min at 100% B; 20.10 min at 100% B; 22.10 min at 1% B; and 27 min at 1% B. A flow rate of 0.3 mL/min was used from 0 min to 20 min and increased to 0.4 mL/min from 20.10 min to 27 min. The column temperature was held at 40 °C and the injection volume used was 5 μL. MS source parameters included: gas temp, 250 °C; gas flow, 9 L/min; nebulizer pressure, 35 psig; sheath gas temp, 250 °C; sheath gas flow, 12 L/min; VCap, 3500 V; and nozzle voltage, 2000 V;: 125V. Agilent MassHunter Profinder 10.0 was used for data analysis with natural isotope abundance correction was performed (Agilent Technologies).

**Data Availability.** All study data are included in the article and/or *SI Appendix*.

**ACKNOWLEDGMENTS.** We thank Elisa de Stanchina and the antitumor assessment core for assistance with tumor xenograft experiments and in vivo tracing experiments. We thank George Sukenick and Rong Wang for assistance with NMR and high resolution mass spectrometry characterization. This work was supported in part by the NIH (R01CA237466 to K.R.K. and P30CA008748 to Memorial Sloan Kettering Cancer Center); the Center for Molecular Imaging and Nanotechnology at Memorial Sloan Kettering Cancer Center (Tow Foundation Postdoctoral Fellowship to R.E.); the Geoffrey Beene Award (to K.R.K. and C.B.T.); and the Thompson Family Foundation (to K.R.K.).

Author affiliations: [a]Department of Radiology, Memorial Sloan Kettering Cancer Center, New York, NY 10065; [b]Molecular Pharmacology Program, Memorial Sloan Kettering Cancer Center, New York, NY 10065; [c]The Donald B. and Catherine C. Marron Cancer Metabolism Center, Memorial Sloan Kettering Cancer Center, New York, NY 10065; [d]Cancer Biology & Genetics Program, Memorial Sloan Kettering Cancer Center, New York, NY 10065; and [e]Weill Cornell Medical College, New York, NY 10065

1. A. Nilsson *et al.*, Quantitative analysis of amino acid metabolism in liver cancer links glutamate excretion to nucleotide synthesis. *Proc. Natl. Acad. Sci. U.S.A.* **117**, 10294–10304 (2020).

2. F. Sanaei Nezhad *et al.*, Quantification of GABA, glutamate and glutamine in a single measurement at 3 T using GABA-edited MEGA-PRESS. *NMR Biomed.* **31**, e3847 (2018).

3. J. Zhang *et al.*, 13C isotope-assisted methods for quantifying glutamine metabolism in cancer cells. *Methods Enzymol.* **542**, 369–389 (2014).
4. H. Yoo, M. R. Antoniewicz, G. Stephanopoulos, J. K. Kelleher, Quantifying reductive carboxylation flux of glutamine to lipid in a brown adipocyte cell line. *J. Biol. Chem.* **283**, 20621–20627 (2008).
5. R. J. DeBerardinis *et al.*, Beyond aerobic glycolysis: Transformed cells can engage in glutamine metabolism that exceeds the requirement for protein and nucleotide synthesis. *Proc. Natl. Acad. Sci. U.S.A.* **104**, 19345–19350 (2007).
6. W. Hu *et al.*, Glutaminase 2, a novel p53 target gene regulating energy metabolism and antioxidant function. *Proc. Natl. Acad. Sci. U.S.A.* **107**, 7455–7460 (2010).
7. S. Suzuki *et al.*, Phosphate-activated glutaminase (GLS2), a p53-inducible regulator of glutamine metabolism and reactive oxygen species. *Proc. Natl. Acad. Sci. U.S.A.* **107**, 7461–7466 (2010).
8. Z. E. Stine, Z. E. Walton, B. J. Altman, A. L. Hsieh, C. V. Dang, MYC, metabolism, and cancer. *Cancer Discov.* **5**, 1024–1039 (2015).
9. D. H. Tran *et al.*, Mitochondrial $NADP^+$ is essential for proline biosynthesis during cell growth. *Nat. Metab.* **3**, 571–585 (2021).
10. J. Zhu *et al.*, Mitochondrial NADP(H) generation is essential for proline biosynthesis. *Science* **372**, 968–972 (2021).
11. B. J. Altman, Z. E. Stine, C. V. Dang, From Krebs to clinic: Glutamine metabolism to cancer therapy. *Nat. Rev. Cancer* **16**, 619–634 (2016).
12. C. Madeira *et al.*, Elevated glutamate and glutamine levels in the cerebrospinal fluid of patients with probable Alzheimer's disease and depression. *Front. Psychiatry* **9**, 561 (2018).
13. A. Daemen *et al.*, Pan-cancer metabolic signature predicts co-dependency on glutaminase and de novo glutathione synthesis linked to a high-mesenchymal cell state. *Cell Metab.* **28**, 383–399.e9 (2018).
14. L. Zhu, K. Ploessl, R. Zhou, D. Mankoff, H. F. Kung, Metabolic imaging of glutamine in cancer. *J. Nucl. Med.* **58**, 533–537 (2017).
15. S. Venneti *et al.*, Glutamine-based PET imaging facilitates enhanced metabolic evaluation of gliomas in vivo. *Sci. Transl. Med.* **7**, 274ra17 (2015).
16. M. P. S. Dunphy *et al.*, In vivo PET assay of tumor glutamine flux and metabolism: In-human trial of $^{18}$F-(2S,4R)-4-fluoroglutamine. *Radiology* **287**, 667–675 (2018).
17. V. Viswanath *et al.*, Kinetic modeling of (18)F-(2S,4R)4-fluoroglutamine in mouse models of breast cancer to estimate glutamine pool size as an indicator of tumor glutamine metabolism. *J. Nucl. Med.* **62**, 1154–1162 (2021).
18. K. Cai *et al.*, Magnetic resonance imaging of glutamate. *Nat. Med.* **18**, 302–306 (2012).
19. K. R. Keshari, D. M. Wilson, Chemistry and biochemistry of 13C hyperpolarized magnetic resonance using dynamic nuclear polarization. *Chem. Soc. Rev.* **43**, 1627–1659 (2014).
20. J. Kurhanewicz *et al.*, Hyperpolarized $^{13}$C MRI: Path to clinical translation in oncology. *Neoplasia* **21**, 1–16 (2019).
21. F. A. Gallagher, M. I. Kettunen, S. E. Day, M. Lerche, K. M. Brindle, 13C MR spectroscopy measurements of glutaminase activity in human hepatocellular carcinoma cells using hyperpolarized 13C-labeled glutamine. *Magn. Reson. Med.* **60**, 253–257 (2008).
22. P. R. Jensen, M. Karlsson, S. Meier, J. O. Duus, M. H. Lerche, Hyperpolarized amino acids for in vivo assays of transaminase activity. *Chemistry* **15**, 10010–10012 (2009).
23. L. Mazuel *et al.*, Intracerebral synthesis of glutamine from hyperpolarized glutamate. *Magn. Reson. Med.* **78**, 1296–1305 (2017).
24. L. Salamanca-Cardona *et al.*, In vivo imaging of glutamine metabolism to the oncometabolite 2-hydroxyglutarate in IDH1/2 mutant tumors. *Cell Metab.* **26**, 830–841.e3 (2017).
25. C. Canapè *et al.*, Probing treatment response of glutaminolytic prostate cancer cells to natural drugs with hyperpolarized [5-(13) C]glutamine. *Magn. Reson. Med.* **73**, 2296–2305 (2015).
26. E. Chiavazza *et al.*, Earth's magnetic field enabled scalar coupling relaxation of 13C nuclei bound to fast-relaxing quadrupolar 14N in amide groups. *J. Magn. Reson.* **227**, 35–38 (2013).
27. J. Son *et al.*, Glutamine supports pancreatic cancer growth through a KRAS-regulated metabolic pathway. *Nature* **496**, 101–105 (2013).
28. S. Mukhopadhyay *et al.*, Undermining glutaminolysis bolsters chemotherapy while NRF2 promotes chemoresistance in KRAS-driven pancreatic cancers. *Cancer Res.* **80**, 1630–1643 (2020).
29. A. Cho, R. Eskandari, K. L. Granlund, K. R. Keshari, Hyperpolarized [6-$^{13}$C,$^{15}N_3$]-arginine as a probe for in vivo arginase activity. *ACS Chem. Biol.* **14**, 665–673 (2019).
30. P. Xu *et al.*, LRH-1-dependent programming of mitochondrial glutamine processing drives liver cancer. *Genes Dev.* **30**, 1255–1260 (2016).
31. D. E. Biancur *et al.*, Compensatory metabolic networks in pancreatic cancers upon perturbation of glutamine metabolism. *Nat. Commun.* **8**, 15965 (2017).
32. W. Qu *et al.*, Facile synthesis [5-(13)C-4-(2)H(2)]-L-glutamine for hyperpolarized MRS imaging of cancer cell metabolism. *Acad. Radiol.* **18**, 932–939 (2011).
33. G. D. Reed *et al.*, High resolution (13)C MRI with hyperpolarized urea: In vivo T(2) mapping and (15)N labeling effects. *IEEE Trans. Med. Imaging* **33**, 362–371 (2014).
34. A. Wibowo, J. M. Park, S. C. Liu, C. Khosla, D. M. Spielman, Real-time in vivo detection of $H_2O_2$ using hyperpolarized $^{13}$C-thiourea. *ACS Chem. Biol.* **12**, 1737–1742 (2017).
35. R. Hata, H. Nonaka, Y. Takakusagi, K. Ichikawa, S. Sando, Design of a hyperpolarized molecular probe for detection of aminopeptidase N activity. *Angew. Chem. Int. Ed. Engl.* **55**, 1765–1768 (2016).
36. D. M. Wilson *et al.*, Generation of hyperpolarized substrates by secondary labeling with [1,1-13C] acetic anhydride. *Proc. Natl. Acad. Sci. U.S.A.* **106**, 5503–5507 (2009).
37. C. R. Bartman *et al.*, Slow TCA flux implies low ATP production in tumors. *bioRxiv* (2021). https://doi.org/10.1101/2021.10.04.463108. Accessed 4 October 2021.
38. N. N. Pavlova, C. B. Thompson, The emerging hallmarks of cancer metabolism. *Cell Metab.* **23**, 27–47 (2016).
39. S. J. Nelson *et al.*, Metabolic imaging of patients with prostate cancer using hyperpolarized [1-(1)(3)C]pyruvate. *Sci. Transl. Med.* **5**, 198ra108 (2013).
40. K. L. Granlund *et al.*, Hyperpolarized MRI of human prostate cancer reveals increased lactate with tumor grade driven by monocarboxylate transporter 1. *Cell Metab.* **31**, 105–114.e3 (2020).
41. F. A. Gallagher *et al.*, Imaging breast cancer using hyperpolarized carbon-13 MRI. *Proc. Natl. Acad. Sci. U.S.A.* **117**, 2092–2098 (2020).
42. V. Z. Miloushev *et al.*, Metabolic imaging of the human brain with hyperpolarized $^{13}$C pyruvate demonstrates $^{13}$C lactate production in brain tumor patients. *Cancer Res.* **78**, 3755–3760 (2018).
43. H. C. Yoo, Y. C. Yu, Y. Sung, J. M. Han, Glutamine reliance in cell metabolism. *Exp. Mol. Med.* **52**, 1496–1516 (2020).
44. B. K. Masisi *et al.*, The role of glutaminase in cancer. *Histopathology* **76**, 498–508 (2020).
45. J. M. Buescher *et al.*, A roadmap for interpreting (13)C metabolite labeling patterns from cells. *Curr. Opin. Biotechnol.* **34**, 189–201 (2015).
46. J. M. Wiseman *et al.*, Desorption electrospray ionization mass spectrometry: Imaging drugs and metabolites in tissues. *Proc. Natl. Acad. Sci. U.S.A.* **105**, 18120–18125 (2008).
47. M. L. Steinhauser *et al.*, Multi-isotope imaging mass spectrometry quantifies stem cell division and metabolism. *Nature* **481**, 516–519 (2012).
48. H. Zeng, Y. Lee, C. Hilty, Quantitative rate determination by dynamic nuclear polarization enhanced NMR of a Diels-Alder reaction. *Anal. Chem.* **82**, 8897–8902 (2010).